Journal of
Experimental and Theoretical Analyses

MDPI

Article

Revealing a New and Significant Thermomechanical Coupling Phenomenon for Rapid Thermal Transients

Florent Clavier [1,2,*], Lionel Desgranges [1] and Christophe Goupil [2]

[1] CEA.DES.IRESNE.DEC, F-13108 St Paul Lez Durance, France; lionel.desgranges@cea.fr
[2] LIED, CNRS, Université Paris Cité, F-75013 Paris, France; christophe.goupil@u-paris.fr
* Correspondence: florent.clavier1122@orange.fr; Tel.: +33-6-70-93-60-87

Abstract

Conventional thermomechanical models recently failed to reproduce the temperature profile measured during rapid annular laser heating of a disk, with discrepancies of up to 150 K. One might have thought that these discrepancies resulted from neglecting the so-called "strong" thermomechanical coupling. However, the discrepancies seemed too large to be explained in this way, suggesting that another more significant phenomenon was involved. In this paper, we first present the laser heating experiment that highlights the failure of conventional models. We then demonstrate that the established strong coupling thermomechanical theory cannot account for the observed divergences, as its impact on temperature does not exceed about 1 K. To address this limitation, we propose a new, more comprehensive thermomechanical coupling formalism based on the thermodynamics of irreversible processes (TIP). Its originality lies in the explicit consideration of spatial strain transport, introduced through the notion of strain flux. This approach reveals a previously unrecognized coupling term representing mechanical work production by heat-to-work conversion. Finally, we provide a quantitative estimate of the influence of this new term by reconsidering the heating experiment. The calculation shows that it could explain the discrepancies between theory and measurement. Although applied here to a specific case, this result supports the validity of our approach. It demonstrates that such coupling must be considered whenever a system is subjected to rapid thermal and mechanical transients.

Keywords: thermomechanical coupling; rapid thermal transients; strain flux; stress gradient; thermodynamics of irreversible processes; heat-to-work conversion

check for updates

Academic Editor: Marco Rossi

Received: 31 July 2025
Revised: 30 September 2025
Accepted: 20 October 2025
Published: 27 October 2025

Citation: Clavier, F.; Desgranges, L.; Goupil, C. Revealing a New and Significant Thermomechanical Coupling Phenomenon for Rapid Thermal Transients. *J. Exp. Theor. Anal.* **2025**, *3*, 33. https://doi.org/10.3390/jeta3040033

Copyright: © 2025 by the authors. Licensee MDPI, Basel, Switzerland. This article is an open access article distributed under the terms and conditions of the Creative Commons Attribution (CC BY) license (https://creativecommons.org/licenses/by/4.0/).

1. Introduction

In many mechanical systems exposed to non-uniform temperature fields, the solid response is often described within a thermomechanical framework based on the "weak coupling" assumption [1]. In this formulation, the thermal field is computed independently of the stress state. This assumption is usually justified by the fact that mechanical effects typically have a negligible influence on the thermal evolution of systems under most practical conditions. Accordingly, the problem reduces to two governing equations [2] as follows:

1. Heat equation

$$\rho c \frac{\partial T}{\partial t} = k \nabla^2 T + r, \tag{1}$$

with ρ the density, c the specific heat, k the thermal conductivity, and r a volumetric heat source.

2. Constitutive law

$$\underline{\underline{\sigma}} = \underline{\underline{\underline{\underline{\mathbb{C}}}}} : \left(\underline{\underline{\varepsilon}} - \underline{\underline{\underline{\underline{\alpha_{th}}}}}\,\Delta T\right), \tag{2}$$

where $\underline{\underline{\sigma}}$ is the Cauchy stress tensor, $\underline{\underline{\underline{\underline{\mathbb{C}}}}}$ is the stiffness tensor, $\underline{\underline{\varepsilon}}$ the strain tensor, $\underline{\underline{\underline{\underline{\alpha_{th}}}}}$ the thermal expansion tensor, and ΔT the temperature increment. : denotes the tensor double contraction.

However, this weak coupling assumption fails under rapid thermal transients. In particular, a team in our laboratory investigated heating conditions representative of a Reactivity Injection Accident (RIA) in cylindrical nuclear fuel (UO_2). To reproduce these situations, a flat cylindrical pellet of (UO_2) is submitted to inhomogeneous heating: the pellet periphery is subjected to abrupt laser-induced heating. The process is fast enough for the temperature of this area to increase abruptly, even before the inside of the pellet has time to heat up. A clear discrepancy between predicted temperature profiles (under weak coupling assumption) and experimental measurements was evidenced [3], Figure 1, thereby questioning the validity of this conventional approach.

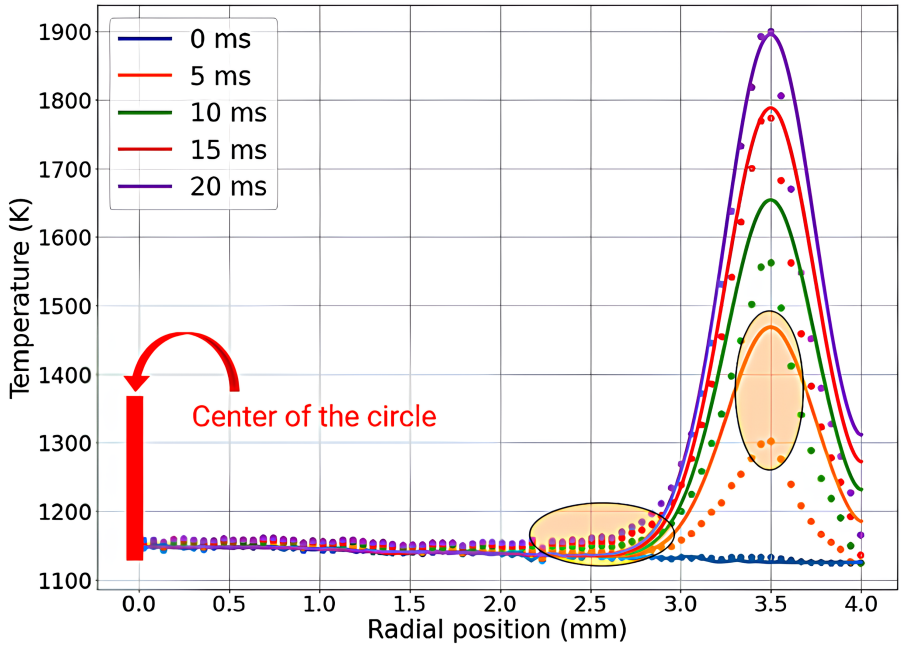


Figure 1. Comparison of simulated (continuous lines) and measured (dots) surface temperature profiles over a duration of 20 ms for a laser heating of 620 W.

The authors who reported these measurements suggested that experimental parameters could contribute to the observed discrepancies. However, their magnitude and the quality of the equipment used [3] suggest that a purely experimental explanation is insufficient. It is therefore legitimate to inquire about a physical origin that would explain these discrepancies, which seem to represent a "heating delay".

One might argue that "strong coupling" theory should correct these errors by justifying the heating delay through a well-known mechanical feedback effect. In Section 2, we quantify the influence that mechanical feedback, as formulated by the strong coupling framework, can exert on temperature for the considered experiment. Our analysis clearly shows that this traditional formalism cannot explain the observed discrepancies.

The particular geometry of laser heating implies that the peripheral ring undergoes thermal expansion while the interior of the pellet has not yet had time to heat up. This situation causes, in the first moments, a stress gradient that drives the propagation of a

deformation wave aimed at mechanically rebalancing the pellet. One can therefore wonder if this deformation flux could actually be coupled to the heat flux and be at the origin of heating delay phenomena. To investigate this, the most obvious approach would seem to be applying the flux coupling theory from thermodynamics of irreversible processes (TIP) to the deformation flux and heat flux.

Currently, existing references on thermomechanical coupling developed within the TIP framework remain local. The mechanical fluxes are identified with the local time derivative $\partial\varepsilon/\partial t$ and the conjugate thermodynamic force with σ/T [4–6]. These formulations, by neglecting spatial transport of deformation and stress gradients, do not account for spatial propagation phenomena. They cannot therefore capture any coupling between heat flux and deformation flux that actually designates propagation. On the other hand, some works propose models that incorporate dependencies on strain gradients $\nabla\boldsymbol{\varepsilon}$. They belong to strain-gradient elasticity theories [7,8]. These models introduce higher-order stresses (hyperstresses) and assume that elastic energy depends on both $\boldsymbol{\varepsilon}$ and its gradient $\nabla\boldsymbol{\varepsilon}$. While effective for size effects and singularity regularization, these models are purely mechanical and do not arise from entropy production principles. They therefore do not belong to TIP and cannot reveal any coupling phenomenon between heat flux and deformation flux.

Thus, in Section 3, we will propose an extended formalism based on TIP that explicitly introduces the notion of deformation propagation. We will therefore address the definition of a deformation flow $\mathbf{J}_{\boldsymbol{\varepsilon}}$ and study its potential coupling with heat flow. We will see that this approach enables the appearance of an additional coupling term, which could cause heating delays during thermal transients. We will also demonstrate that this could quantitatively explain the temperature discrepancies observed during the heating experiment presented above.

2. Strong Coupling Formalism Approach

2.1. Observation of Heating Delay and Calculation of Corresponding Energy

In Figure 1, pronounced discrepancies between the measured and simulated temperature profiles are evident. In particular, within the core of the directly heated zone, the temperature rises more slowly than predicted by the simulation. The largest discrepancy occurs at the center of the heated zone (3.5 mm) at 5 ms, with a difference of approximately 150 K between the simulation and the experimental measurement.

Considering a specific heat capacity of $c^{UO_2} \approx 370\,\mathrm{J\,kg^{-1}\,K^{-1}}$ and a density of $\rho^{UO_2} \approx 11\,\mathrm{g\,cm^{-3}}$ [9], this temperature difference $\Delta T \approx 150\,\mathrm{K}$ corresponds to a missing volumetric energy density of approximately

$$e_{\text{missing}} \approx 0.5\,\mathrm{J\,mm^{-3}}. \tag{3}$$

2.2. Theoretical Framework of Strong Thermomechanical Coupling

Adopting a theoretical framework of strong thermomechanical coupling requires explicitly accounting for the mechanical influence on thermal behavior [10]. Within this context, and based on the constitutive laws of solids at equilibrium, the aim is to derive a comprehensive heat equation that incorporates mechanical feedback.

The fuel pellet is modeled as a continuous and homogeneous medium subjected only to thermal and mechanical variations. No mass exchange, chemical reaction, or charge transport is considered. The analysis assumes infinitesimal deformations and the validity of the local equilibrium hypothesis so that the thermodynamic state variables remain well defined at each point of the material. At the boundary, the solid is subjected to a heat flux imposed by the laser (Neumann boundary condition). It is not subjected to mechanical forces coming from the outside, but, as we have seen, the heating geometry

implies mechanical forces. Under these conditions, the local internal energy balance can thus be expressed as

$$\rho \frac{\partial e}{\partial t} = \underline{\underline{\sigma}} : \underline{\underline{D}} + r - \nabla \cdot \underline{q}, \tag{4}$$

where ρ is the density, e the specific internal energy, $\underline{\underline{\sigma}}$ the Cauchy stress tensor, $\underline{\underline{D}}$ the strain rate tensor, r a volumetric energy source, and $\underline{q}$ the heat flux vector.

Under the assumption of infinitesimal deformations and following the local state approach, the strain reduces to the linearized strain tensor $\underline{\underline{\varepsilon}}$, such that $\underline{\underline{D}} = \partial \underline{\underline{\varepsilon}} / \partial t$. The total strain tensor can be decomposed into thermoelastic and plastic contributions

$$\underline{\underline{\varepsilon}} = \underline{\underline{\varepsilon}}^e + \underline{\underline{\varepsilon}}^p. \tag{5}$$

Introducing the Helmholtz free energy $\psi = e - Ts$ as the thermodynamic potential, where s is the specific entropy and T the temperature, and applying the Clausius–Duhem inequality, the following constitutive relations are obtained

$$\underline{\underline{\sigma}} = \rho \frac{\partial \psi}{\partial \underline{\underline{\varepsilon}}^e}, \quad s = -\frac{\partial \psi}{\partial T}. \tag{6}$$

Details regarding the choice of independent variables to express ψ are provided in Appendix A.

Without detailing the derivation (such derivations are provided in [10]), the above considerations finally lead to the heat equation in the framework of strong thermomechanical coupling

$$\rho c_{\varepsilon^e} \frac{\partial T}{\partial t} = T \frac{\partial \underline{\underline{\sigma}}}{\partial T} : \frac{\partial \underline{\underline{\varepsilon}}^e}{\partial t} + \underline{\underline{\sigma}} : \frac{\partial \underline{\underline{\varepsilon}}^p}{\partial t} + r - \operatorname{div} \underline{q} \tag{7}$$

where the following apply:

- $c_{\varepsilon^e} = -T \frac{\partial^2 \psi}{\partial T^2}$ is the heat capacity at constant thermoelastic strain,
- $\frac{\partial \underline{\underline{\sigma}}}{\partial T} = \rho \frac{\partial^2 \psi}{\partial T \partial \underline{\underline{\varepsilon}}^e}$ is the stress sensitivity to temperature,
- $\underline{\underline{\sigma}} : \frac{\partial \underline{\underline{\varepsilon}}^p}{\partial t}$ is the mechanical dissipation.

For thermodynamic consistency, several restrictions delimit the applicability of the present formulation: (i) the heat capacity c_{ε^e} is strictly positive, (ii) the thermal conductivity (implicit in Fourier's law $\underline{q} = -k \nabla T$) must be positive definite, (iii) the elasticity tensor derived from $\partial \underline{\underline{\sigma}} / \partial \underline{\underline{\varepsilon}}^e = \partial^2 \psi / \partial (\underline{\underline{\varepsilon}}^e)^2$ is positive definite, ensuring stability, and (iv) the plastic dissipation $\underline{\underline{\sigma}} : \dot{\underline{\underline{\varepsilon}}}^p \geq 0$ in accordance with the second law.

This extended heat equation introduces several terms that are typically neglected in standard thermomechanical models based on the weak coupling assumption. Notably, the term

$$T \frac{\partial \underline{\underline{\sigma}}}{\partial T} : \frac{\partial \underline{\underline{\varepsilon}}^e}{\partial t} \tag{8}$$

represents thermoelastic coupling, i.e., the influence of reversible elastic deformation on the thermal response. Within the framework of the present study, this is the only term that could plausibly account for the observed energy deficit.

Conversely, the term

$$\underline{\underline{\sigma}} : \frac{\partial \underline{\underline{\varepsilon}}^p}{\partial t}, \tag{9}$$

which corresponds to mechanical dissipation, cannot explain the discrepancy, as it solely contributes to heating. Moreover, under the thermal and mechanical conditions experienced by the pellet during the first 5 ms, plastic effects are negligible.

Accordingly, in the following section, we estimate the order of magnitude of the energy potentially associated with the thermoelastic coupling term

$$T\frac{\partial \underline{\underline{\sigma}}}{\partial T} : \frac{\partial \underline{\underline{\varepsilon}}^e}{\partial t}. \tag{10}$$

2.3. Quantification of the Energy Associated with Thermoelastic Coupling

Under the linear thermoelastic assumption, Hooke's law implies that the sensitivity of stress to temperature can be expressed as

$$\frac{\partial \underline{\underline{\sigma}}}{\partial T} = -\underline{\underline{\underline{\underline{\mathbb{C}}}}} : \frac{\partial \underline{\underline{\varepsilon}}^e}{\partial T} = -\underline{\underline{\underline{\underline{\mathbb{C}}}}} : \underline{\underline{\underline{\underline{\alpha_{\text{th}}}}}}. \tag{11}$$

The objective is to estimate the order of magnitude of the energy contribution associated with the thermoelastic coupling term. To simplify the calculation, the tensorial formulation can be approximated by a scalar representation, yielding a first estimate of the internal volumetric energy variation due solely to thermoelastic effects

$$\frac{\partial e_{\text{th-el}}}{\partial t} \approx T\,(-E\,\alpha_{\text{th}})\frac{\partial \epsilon}{\partial t}, \tag{12}$$

where E is the Young's modulus and $\epsilon = \delta V / V_0$ is the relative volumetric strain.

To maximize the estimate of $e_{\text{th-el}}$ at $t = 5$ ms, we assume purely thermoelastic deformation and free expansion of the peripheral ring, i.e., $\frac{\partial \epsilon}{\partial t} = \alpha_{\text{th}}\,\frac{\partial T}{\partial t}$. This leads to

$$e_{\text{th-el}}^{5\,\text{ms, MAX}} \approx \int_0^{5\,\text{ms}} -T\,E\,\alpha_{\text{th}}^2\,\frac{\partial T}{\partial t}\,dt. \tag{13}$$

Assuming E and α_{th} are constant over the interval, the integral simplifies to

$$e_{\text{th-el}}^{5\,\text{ms, MAX}} \approx -E\,\alpha_{\text{th}}^2\left[\frac{T(t)^2}{2}\right]_0^{5\,\text{ms}}. \tag{14}$$

For the numerical evaluation, we consider uranium dioxide at approximately 1300 K [9]: $E^{UO_2} \approx 200$ GPa and $\alpha_{\text{th}}^{UO_2} \approx 10^{-5}$ K^{-1}. From Figure 1, the temperature at the center of the heated zone rises from $T(t_0) \approx 1130$ K to $T(t = 5\text{ ms}) \approx 1300$ K. The resulting energy estimate is

$$e_{\text{th-el}}^{5\,\text{ms, MAX}} \approx= -4 \times 10^{-3}\,\text{J/mm}^3. \tag{15}$$

Despite employing strong approximations intended to maximize the influence of the thermoelastic coupling in the classical sense, the magnitude of $\left|e_{\text{th-el}}^{5\,\text{ms}}\right|$ remains orders of magnitude smaller than the observed missing energy density, $e_{\text{missing}} \approx 0.5$ J/mm^3. Therefore, the energy deficit observed in the heated zone cannot be attributed solely to the absence of strong thermomechanical coupling as conventionally understood.

Having established that the conventional theory of strong coupling cannot explain the observed discrepancies, we now turn to the development of a more comprehensive thermomechanical coupling framework. Based on the thermodynamics of irreversible processes, it explicitly takes into account spatial transport phenomena that are neglected in traditional approaches.

3. Thermomechanical Coupling Based on the Thermodynamics of Irreversible Processes

The thermodynamics of irreversible processes (TIP) provides a rigorous framework for analyzing systems evolving out of equilibrium. Unlike classical thermodynamics, which focuses on reversible transformations and equilibrium states, TIP addresses transport phenomena and dissipative processes, making it particularly suited for studying coupled irreversible mechanisms in our system.

Through our work, we adopt the local equilibrium hypothesis, a cornerstone of TIP, which assumes that each infinitesimal volume element is locally at thermodynamic equilibrium, even if the system as a whole is not [11]. This allows the definition of local intensive quantities and the application of equilibrium relations while accounting for macroscopic gradients and fluxes. Appendix B.1 provides a justification for its validity in fast transient phenomena, demonstrating that microscopic relaxation times remain much shorter than the macroscopic timescales of interest.

Our analysis is restricted to thermoelastic deformations, neglecting plastic effects. Existing thermomechanical coupling laws already provide comprehensive formulations for plasticity-related heat transfer, which are outside the scope of the present study. This restriction allows focusing on the development of a new theoretical framework for thermoelastic coupling. We also place our study within the context of continuum mechanics.

For clarity, all tensorial quantities (order ≥ 1) are denoted in **boldface**, with their rank specified upon introduction. Appendix B.2 details the full notational conventions, including tensor products and special tensors.

3.1. Energy and Entropy Balances

The internal energy balance remains

$$\rho \frac{\partial e}{\partial t} = \boldsymbol{\sigma} : \boldsymbol{D} + r - \nabla \cdot \mathbf{J}_q, \tag{16}$$

but TIP emphasizes entropy exchanges and production. Thus, let $S(t)$ denote the total system entropy and $s(\mathbf{r}, t)$ the local entropy per unit volume

$$S(t) = \int_V s(\mathbf{r}, t)\, dV. \tag{17}$$

The local thermodynamic identity, ensured by the local equilibrium hypothesis, reads

$$du = T\, ds + \boldsymbol{\sigma} : d\boldsymbol{\epsilon}, \quad u = u(s, \boldsymbol{\epsilon}), \tag{18}$$

which expresses the differential variation in internal energy in terms of local entropy and strain, forming the basis for deriving entropy production and coupling laws.

3.2. Entropy Production

The local entropy evolves according to

$$\frac{\partial s(\mathbf{r}, t)}{\partial t} = -\nabla \cdot \mathbf{J}_s + \nu_s, \tag{19}$$

where $\mathbf{J}_s$ is the entropy flux and $\nu_s \geq 0$ is the local entropy production.

The entropy production density, derived in Appendix B.3, is

$$\nu_s = \nabla I_u \cdot \mathbf{J}_u + \nabla \boldsymbol{I}_{\boldsymbol{\epsilon}} \vdots \mathbf{J}_{\boldsymbol{\epsilon}}, \tag{20}$$

with $I_u = \left(\frac{\partial s}{\partial u}\right)_{\boldsymbol{\epsilon}}$, $\boldsymbol{I}_{\boldsymbol{\epsilon}} = \left(\frac{\partial s}{\partial \boldsymbol{\epsilon}}\right)_u$, and $\mathbf{J}_u$ the energy flux density.

As previously mentioned, part of the originality of this work lies in the introduction and consideration of the strain flux density $\mathbf{J}_{\boldsymbol{\epsilon}}$. When a system is subjected to mechanical constraints, stress and strain propagate through the material. For instance, compression of a spring generates stress changes in regions remote from the applied load. The strain flux $\mathbf{J}_{\boldsymbol{\epsilon}}$ represents the spatial transport of local strain. Concretely, it is an order 3 tensor, and each component $J_{\epsilon_{ij,k}}$ represents the flux of the strain component ϵ_{ij} in the direction k. The unit of $\mathbf{J}_{\boldsymbol{\epsilon}}$ is $\mathrm{m} \cdot \mathrm{s}^{-1}$ (dilation flux in $\mathrm{m}^3 \cdot \mathrm{m}^{-2} \cdot \mathrm{s}^{-1}$). In the continuous framework considered here, this flux satisfies the local conservation equation

$$\frac{\partial \boldsymbol{\epsilon}}{\partial t} + \nabla \cdot \mathbf{J}_{\boldsymbol{\epsilon}} = \mathbb{O}^{(2)}, \tag{21}$$

where the divergence is applied to the third index of $\mathbf{J}_{\boldsymbol{\epsilon}}$.

This relation expresses that the local temporal variations in the strain are balanced by spatial transport, consistent with the interpretation of the flux as a mechanism for the propagation of elastic deformations.

Then, defining $\mathbf{F}_u = \nabla I_u$ and $\mathbf{F}_{\boldsymbol{\epsilon}} = \nabla \boldsymbol{I}_{\boldsymbol{\epsilon}}$ as thermodynamic forces, we obtain the canonical force-flux form

$$\nu_s = \mathbf{F}_u \cdot \mathbf{J}_u + \mathbf{F}_{\boldsymbol{\epsilon}} \vdots \mathbf{J}_{\boldsymbol{\epsilon}}, \tag{22}$$

expressing that entropy production arises from gradients of intensive quantities driving fluxes that restore equilibrium.

3.3. Determination of Thermodynamic Forces

From Equation (18), the differential of entropy is

$$ds = \frac{1}{T}\, du - \frac{\boldsymbol{\sigma}}{T} : d\boldsymbol{\epsilon}, \tag{23}$$

yielding

$$\mathbf{F}_u = \nabla\left(\frac{1}{T}\right), \quad \mathbf{F}_{\boldsymbol{\epsilon}} = \nabla\left(-\frac{\boldsymbol{\sigma}}{T}\right). \tag{24}$$

The entropy production then reads

$$\nu_s = \nabla\left(\frac{1}{T}\right) \cdot \mathbf{J}_u + \nabla\left(-\frac{\boldsymbol{\sigma}}{T}\right) \vdots \mathbf{J}_{\boldsymbol{\epsilon}}. \tag{25}$$

Expressed in the heat/strain basis $(\boldsymbol{q}, \boldsymbol{\epsilon})$, as detailed in Appendix B.4, we have

$$\nu_s = \nabla\left(\frac{1}{T}\right) \cdot \mathbf{J}_q - \frac{1}{T}(\nabla \boldsymbol{\sigma}) \vdots \mathbf{J}_{\boldsymbol{\epsilon}}, \tag{26}$$

and the associated thermodynamic forces are

$$\mathbf{F}_q = \nabla\left(\frac{1}{T}\right), \quad \mathbf{F}_{\boldsymbol{\epsilon}} = -\frac{1}{T}(\nabla \boldsymbol{\sigma}). \tag{27}$$

3.4. Linear Phenomenological Relations

Assuming small deviations from equilibrium, the fluxes can be linearized as

$$\mathbf{J}_i = \sum_j \mathbf{L}_{ij} \cdot \mathbf{F}_j, \tag{28}$$

where $\mathbf{L}_{ij}$ are the Onsager phenomenological coefficients.

The diagonal coefficients describe direct effects, while the off-diagonal terms represent coupling effects. In the thermomechanical context

$$\mathbf{J}_q = \mathbf{L}_{qq} \cdot \nabla\left(\frac{1}{T}\right) + \mathbf{L}_{q\boldsymbol{\epsilon}} \vdots \left(-\frac{1}{T}\nabla\boldsymbol{\sigma}\right), \tag{29}$$

$$\mathbf{J}_{\boldsymbol{\epsilon}} = \mathbf{L}_{\boldsymbol{\epsilon}q} \cdot \nabla\left(\frac{1}{T}\right) + \mathbf{L}_{\boldsymbol{\epsilon}\boldsymbol{\epsilon}} \vdots \left(-\frac{1}{T}\nabla\boldsymbol{\sigma}\right), \tag{30}$$

where $\mathbf{L}_{qq}$ is a second-order tensor, $\mathbf{L}_{q\boldsymbol{\epsilon}}$ and $\mathbf{L}_{\boldsymbol{\epsilon}q}$ are fourth-order tensors, and $\mathbf{L}_{\boldsymbol{\epsilon}\boldsymbol{\epsilon}}$ is a sixth-order tensor. According to the Onsager reciprocal relations [12,13], $\mathbf{L}_{q\boldsymbol{\epsilon}} = \mathbf{L}_{\boldsymbol{\epsilon}q}$.

To be consistent with the second law of thermodynamics, these material constants must satisfy the following restrictions:

- $\mathbf{L}_{qq}$, $\mathbf{L}_{\boldsymbol{\epsilon}\boldsymbol{\epsilon}}$ must be positive semi-definite tensors;
- and the quadratic form of entropy production

$$\sigma_s = \nabla\left(\tfrac{1}{T}\right) \cdot \mathbf{L}_{qq} \cdot \nabla\left(\tfrac{1}{T}\right) + 2\,\nabla\left(\tfrac{1}{T}\right) \cdot \mathbf{L}_{q\boldsymbol{\epsilon}} \vdots \left(-\tfrac{1}{T}\nabla\boldsymbol{\sigma}\right) + \left(-\tfrac{1}{T}\nabla\boldsymbol{\sigma}\right) \vdots \mathbf{L}_{\boldsymbol{\epsilon}\boldsymbol{\epsilon}} \vdots \left(-\tfrac{1}{T}\nabla\boldsymbol{\sigma}\right),$$

must be non-negative for all admissible processes ($\sigma_s \geq 0$);

3.5. Extension to Non-Stationary Situations and Finite Propagation Speeds

The developments above have been restricted to stationary or quasi-stationary situations, in which the linear phenomenological relations of Onsager apply directly. However, in many systems involving very fast transients, memory effects and finite propagation speeds must be taken into account. Several works have seriously studied this question, particularly examining the impact of memory effects and finite propagation speeds on wave propagation in thermoelastic media [14,15]. These theories are entirely compatible with the TIP formalism. Indeed, in 1961, Zwanzig [16] generalized Onsager's framework by introducing convolution relations between fluxes and thermodynamic forces. He therefore incorporated temporal correlations between past states of the system and its present response

$$\mathbf{J}_i(t) = \sum_j \int_0^t \mathbf{L}_{ij}(t-s)\,\mathbf{F}_j(s)\,ds, \tag{31}$$

where $\mathbf{L}_{ij}(t-s)$ is a memory kernel characterizing the relaxation of flux $\mathbf{J}_i$ under force $\mathbf{F}_j$.

3.5.1. Cattaneo–Vernotte Formulation

For the case of heat conduction, choosing an exponential kernel [16] for $\mathbf{L}_{qq}(t-s)$ leads to the so-called Cattaneo–Vernotte equation [17,18]

$$\tau\frac{\partial \mathbf{J}_q}{\partial t} + \mathbf{J}_q = -k\nabla T, \tag{32}$$

which introduces a finite thermal relaxation time τ.

Physically, this means that the heat flux does not adjust instantaneously to a temperature gradient but rather relaxes with a characteristic delay. This delay originates from the finite time required for microscopic energy carriers (e.g., phonons or electrons) to relax toward local equilibrium after a perturbation.

This modification is directly connected to the principle of the local equilibrium hypothesis. Fourier's law assumes that microscopic equilibration occurs on timescales much shorter than macroscopic variations, such that the heat flux is always locally equilibrated. When τ becomes comparable to the observation timescale, the system cannot be described as being in local equilibrium at every instant, and memory terms must be retained.

The same situation arises in mechanics: Hooke's law assumes instantaneous stress–strain adjustment, while some models (Maxwell, Kelvin–Voigt, and Zener) introduce relaxation times and memory kernels [19]. In this context, the mechanical flux (strain rate) responds to the thermodynamic force (stress gradient) with finite delay, in direct analogy with the Cattaneo–Vernotte correction for heat flux.

3.5.2. Relevance to Our Study

In the case of the considered laser heating experiment, the divergences appear for times of the order of 1–10 ms. These are many orders of magnitude larger than the microscopic relaxation times governing local equilibration, whether thermal (nanosecond to microsecond time scales) or mechanical (rather 10 to 100 picoseconds) [20]. Consequently, the macroscopic evolution of the system is well described within the framework of TIP under the local equilibrium hypothesis, with constant Onsager coefficients and without explicit memory effects. Although these generalizations are of theoretical and experimental interest, they remain confined to ultrafast phenomena (picosecond to microsecond regimes) and are irrelevant for the processes studied here.

We therefore conclude that the coupled phenomenological relations

$$\mathbf{J}_q = \mathbf{L}_{qq} \cdot \nabla\left(\frac{1}{T}\right) + \mathbf{L}_{q\boldsymbol{\epsilon}} \vdots \left(-\frac{1}{T}\nabla\boldsymbol{\sigma}\right), \tag{33}$$

$$\mathbf{J}_{\boldsymbol{\epsilon}} = \mathbf{L}_{\boldsymbol{\epsilon}q} \cdot \nabla\left(\frac{1}{T}\right) + \mathbf{L}_{\boldsymbol{\epsilon}\boldsymbol{\epsilon}} \vdots \left(-\frac{1}{T}\nabla\boldsymbol{\sigma}\right), \tag{34}$$

with constant Onsager phenomenological coefficients, provide the appropriate description of thermomechanical coupling in our work.

3.6. Decomposition of the Heat Flux

To elucidate the mechanisms underlying the thermomechanical coupling and the observed heating delay, it is instructive to rewrite the heat flux in Equation (29) as the sum of two physically distinct contributions. The detailed derivation, which involves setting the strain flux to zero and manipulating the kinetic coefficients, is provided in Appendix B.5. This yields the following structure:

$$\mathbf{J}_q = \underbrace{-\boldsymbol{\kappa}_{\boldsymbol{\epsilon}} \cdot \nabla T}_{\text{classical heat conduction}} + \underbrace{\boldsymbol{\Pi} \vdots \mathbf{J}_{\boldsymbol{\epsilon}}}_{\text{mechanically induced heat transport}}, \tag{35}$$

where $\boldsymbol{\kappa}_{\boldsymbol{\epsilon}}$ denotes the thermal conductivity tensor in the absence of strain flux, and $\boldsymbol{\Pi} = \mathbf{L}_{q\boldsymbol{\epsilon}} \vdots \mathbf{L}_{\boldsymbol{\epsilon}\boldsymbol{\epsilon}}^{-1}$ represents the coupling tensor relating strain flux to heat flux. The first term corresponds to standard Fourier conduction, independent of any mechanical transport, while the second term accounts for heat carried by purely mechanical motion.

It is equally crucial to distinguish between microscopic relaxation times, discussed previously, and the macroscopic characteristic times of thermal and mechanical responses. The former describes the equilibration of microscopic degrees of freedom (phonons, electrons, dislocations, etc.), typically on ultrafast timescales. In contrast, macroscopic characteristic times govern the observable evolution of temperature and strain fields at the continuum scale. These times are dictated by transport coefficients, boundary conditions, and geometric dimensions, and they control how the system evolves at the observable level.

From this macroscopic perspective, both the thermal response time τ_{th} and the mechanical response time τ_{me} are of central importance. One is associated with the diffusion of heat through the material, while the other corresponds to the propagation and equilibration of mechanical deformations. In solids, thermal diffusion occurs much more slowly than

the propagation of elastic waves and the establishment of mechanical equilibrium, so that $\tau_{\text{th}} \gg \tau_{\text{me}}$. This clear separation of timescales implies that, during transient dynamics, the thermal response governs the overall system evolution. The mechanical fields can therefore be regarded as adapting quasi-instantaneously to the evolving thermal state.

In terms of fluxes, this means that the strain flux $\mathbf{J}_{\boldsymbol{\epsilon}}$ reaches its maximum almost immediately at the onset of the transient, before relaxing to zero as steady state is approached. Indeed, since $\tau_{\text{th}} \gg \tau_{\text{me}}$, $\mathbf{J}_{\boldsymbol{\epsilon}}$ is directly proportional to the temporal derivative of the thermal expansion of the heated area. And the latter is at its maximum at the very beginning of the transient. As a consequence, it is precisely during these very early instants that the thermal evolution is most strongly influenced by the mechanically induced feedback term $\boldsymbol{\Pi} \vdots \mathbf{J}_{\boldsymbol{\epsilon}}$ in Equation (35).

3.7. Determination of the Coupling Tensor $\boldsymbol{\Pi}$

In order to determine the coupling tensor $\boldsymbol{\Pi}$ introduced in Equation (35), we must first clarify the nature of the stresses considered in our formulation.

In classical continuum mechanics theory, the constitutive relation is usually written as

$$d\boldsymbol{\sigma} = \mathbf{C} : (d\boldsymbol{\epsilon} - \boldsymbol{\alpha}_{\text{th}}\, dT), \tag{36}$$

where $\mathbf{C}$ is the stiffness tensor, $\boldsymbol{\alpha}_{\text{th}}$ the thermal expansion tensor, and dT the temperature variation. This relation already embodies a form of thermomechanical coupling, widely documented in the literature.

However, to remain consistent with our approach, it is essential to separate purely mechanical stresses from thermally induced stresses. The stresses $\boldsymbol{\sigma}$ appearing in our kinetic formulation correspond exclusively to mechanical contributions

$$d\boldsymbol{\sigma} = d\boldsymbol{\sigma}_{\text{me}} = \mathbf{C} : d\boldsymbol{\epsilon}. \tag{37}$$

The additional stress arising purely from thermal effects is denoted $\boldsymbol{\sigma}_{\text{th}}$, with

$$d\boldsymbol{\sigma}_{\text{th}} = -\mathbf{C} : \boldsymbol{\alpha}_{\text{th}}\, dT. \tag{38}$$

When a system approaches the steady state, the temperature stops changing, and the gradients of thermal and mechanical stresses must exactly balance each other. Locally, this reads

$$\nabla\boldsymbol{\sigma}_{\text{me}} = -\nabla\boldsymbol{\sigma}_{\text{th}}. \tag{39}$$

Substituting the definition of $\boldsymbol{\sigma}_{\text{th}}$, we obtain

$$\nabla\boldsymbol{\sigma}_{\text{me}} = \mathbf{C} : \boldsymbol{\alpha}_{\text{th}} \otimes \nabla T. \tag{40}$$

Moreover, at steady state, the strain flux $\mathbf{J}_{\boldsymbol{\epsilon}}$ vanishes. As shown in Appendix B.6, this condition combined with Equation (40) constrains the Onsager coefficients, leading to

$$\mathbf{L}_{\boldsymbol{\epsilon} q} = -T(\mathbf{C} : \boldsymbol{\alpha}_{\text{th}}) : \mathbf{L}_{\boldsymbol{\epsilon}\boldsymbol{\epsilon}}. \tag{41}$$

Consequently, the coupling tensor defined in Equation (35) becomes

$$\boldsymbol{\Pi} = \mathbf{L}_{q\boldsymbol{\epsilon}} \vdots \mathbf{L}_{\boldsymbol{\epsilon}\boldsymbol{\epsilon}}^{-1} = -T(\mathbf{C} : \boldsymbol{\alpha}_{\text{th}}) : \mathbb{I}^{(6)}. \tag{42}$$

This explicit identification highlights the fact that $\boldsymbol{\Pi}$ originates from the interplay between elasticity and thermal expansion.

3.8. Origin of the Heating Delay

3.8.1. Sources of Heat Emission and Absorption

Knowing now the expression of $\boldsymbol{\Pi}$, the heat flux Equation (35) can be rewritten in terms of known physical parameters

$$\mathbf{J}_q = -\boldsymbol{\kappa}_{\boldsymbol{\epsilon}} \cdot \nabla T - T \cdot (\mathbf{C} : \boldsymbol{\alpha}_{\text{th}}) : \mathbf{J}_{\boldsymbol{\epsilon}}. \tag{43}$$

To assess in detail the different sources of heat emission or absorption, it is necessary to evaluate the divergence $\nabla \cdot \mathbf{J}_q$. Without considering the temperature dependence of $\mathbf{C}$ and $\boldsymbol{\alpha}_{\text{th}}$, the divergence can be written as

$$\nabla \cdot \mathbf{J}_q = \nabla \cdot [-\boldsymbol{\kappa}_{\boldsymbol{\epsilon}} \cdot \nabla T] - T \cdot (\mathbf{C} : \boldsymbol{\alpha}_{\text{th}}) : (\nabla \cdot \mathbf{J}_{\boldsymbol{\epsilon}}) - \nabla T \cdot (\mathbf{C} : \boldsymbol{\alpha}_{\text{th}}) : \mathbf{J}_{\boldsymbol{\epsilon}}. \tag{44}$$

This decomposition highlights three distinct contributions. The first two are known and allow us to confirm the compatibility of our approach with others, and they are presented as follows:

1. Pure thermal conduction: The term $\nabla \cdot [-\boldsymbol{\kappa}_{\boldsymbol{\epsilon}} \cdot \nabla T]$ represents the power released by classical thermal conduction, corresponding to Fourier's law in the absence of mechanical transport. It is equivalent to what is called div $\underline{q}$ in the heat Equation (7).

2. Strong thermoelastic coupling: The term $T \cdot (\mathbf{C} : \boldsymbol{\alpha}_{\text{th}}) : (\nabla \cdot \mathbf{J}_{\boldsymbol{\epsilon}})$ corresponds exactly to the thermoelastic coupling term $T \frac{\partial \underline{\underline{\sigma}}}{\partial T} : \frac{\partial \underline{\underline{\epsilon}}^e}{\partial t}$ that appears in Equation (7), which was of particular interest in our strong coupling approach. This term quantifies the heat associated with thermoelastic contractions and expansions.

The third term $\nabla T \cdot (\mathbf{C} : \boldsymbol{\alpha}_{\text{th}}) : \mathbf{J}_{\boldsymbol{\epsilon}}$, however, is completely new. Studying it, we notice that it represents mechanical work production by heat-to-work conversion in the presence of a temperature gradient. It describes the energy supplied by heat to $\mathbf{J}_{\boldsymbol{\epsilon}}$ to induce boundary displacements during its propagation. We provide a more detailed analysis of this phenomenon in Appendix C. Basically, the presence of $\mathbf{J}_{\boldsymbol{\epsilon}}$ signifies not only the transfer of heat but also the concomitant production in mechanical work associated with the establishment of the stress field. Accordingly, during the short initial regime where $\mathbf{J}_{\boldsymbol{\epsilon}}$ is at its maximum, a fraction of the incident thermal energy is irreversibly converted into mechanical work. The system thus operates transiently as a diathermal heat engine.

This latest and newest coupling term bears a strong formal resemblance to the thermoelectric case. Indeed, in thermoelectricity, a heat flux $\mathbf{J}_q$ interacting with an electric current $\mathbf{J}_e$ in the presence of a temperature gradient leads to electrical work production. In this context, the term $\nabla T \cdot \alpha \, \mathbf{J}_e$ (with α being the Seebeck coefficient) quantifies the power generated by thermoelectric conversion [21]. Here, a similar coupling arises between the strain flux and the thermal gradient, leading to mechanical work production through purely thermomechanical means.

3.8.2. Physical Meaning for Rapid Thermal Transients

This new coupling term is all the more important for phenomena studied over times between τ_{th} and τ_{me}. Rapid thermal transients such as the laser heating experiment mentioned above are perfect examples of this. Taking this new coupling term into account, we now understand that the spatial and temporal distribution of temperature may actually differ from that predicted by conventional thermomechanical simulations, which neglect this effect.

If we refer back to Figure 1 showing the differences between the simulated temperature profile and the temperature profile measured during the laser heating experiment, the term $\nabla(T) \cdot (\mathbf{C} : \boldsymbol{\alpha}_{\text{th}}) : \mathbf{J}_{\boldsymbol{\epsilon}}$ could explain the delay in heating observed at the center of the heated zone at the start of the transient. Indeed, it is from this zone that the flux $\mathbf{J}_{\boldsymbol{\epsilon}}$ (maximal at the

very beginning of the transient) propagates toward the center, crossing the thermal gradient zone where it participates in the conversion of thermal energy into mechanical work. This conversion acts as cooling, which, in the context of heating, manifests as a slowing of the heating process.

We have just explained that the flux $\mathbf{J}_\epsilon$ originates from the periphery and propagates toward the center of the pellet. To justify this statement, it is necessary to specify the boundary conditions concerning this flux. Previously, we have detailed the notion of deformation flux and written the associated conservation Equation (21). This clearly defines the divergence of $\mathbf{J}_\epsilon$, and thus defines it up to a constant. To determine its absolute value, we must establish its value at the system's interfaces with the exterior. This can be achieved by applying the Green–Ostrogradsky formula. In the case of laser heating, it suffices to determine its value at the cylindrical surface (interface with the exterior). The Green–Ostrogradsky formula allows us to write

$$\int_{\partial V} \mathbf{J}_\epsilon \cdot d\mathbf{S} = \int_V \nabla \cdot \mathbf{J}_\epsilon \, dV. \tag{45}$$

From Equation (21), $\nabla \cdot \mathbf{J}_\epsilon = -\frac{\partial \epsilon}{\partial t}$. Moreover, the system has rotational symmetry, so $\mathbf{J}_\epsilon$ can be considered uniform over the entire cylindrical surface. Finally, the propagation $\mathbf{J}_\epsilon$ is collinear (and opposite) to $\vec{dS}$ because it results precisely from a dilation of the cylinder along radial directions. Details on this "collinearity" are given in Appendix D. Finally, Equation (45) becomes

$$-\mathbf{J}_{\epsilon,\text{boundary}} \cdot S_{\text{cylindrical}} = \int_V \left(-\frac{\partial \epsilon}{\partial t} \right) dV, \tag{46}$$

and thus,

$$\mathbf{J}_{\epsilon,\text{boundary}} = \frac{1}{S_{\text{cylindrical}}} \int_V \frac{\partial \epsilon}{\partial t} \, dV. \tag{47}$$

The boundary conditions are thus defined, and we have access to the boundary value that was necessary to have a complete definition of the flux $\mathbf{J}_\epsilon$.

3.8.3. Quantitative Estimate of the New Coupling Term

We have shown that this new coupling term can qualitatively explain heating delays. Now, we want to draw on the laser heating experiment to evaluate whether the energy density $e^{5\,\text{ms}}_{\text{conversion}}$ represented by the coupling term over the early transient $0 \leq t \leq t_f$ (with $t_f = 5$ ms)

$$e^{5\,\text{ms}}_{\text{conversion}} = \int_0^{t_f} \nabla T \cdot (\mathbf{C} : \boldsymbol{\alpha}_{\text{th}}) : \mathbf{J}_\epsilon(t) \, dt \tag{48}$$

could quantitatively explain the observed heating delay.

We have limited means and information, so this is an approximate calculation whose main objective is to give us orders of magnitude. A first difficulty is to clearly identify and measure the deformation flux $\mathbf{J}_\epsilon$. To remedy this, we can use a simplifying assumption that considers this flux constant over the first 5 ms and takes this constant as the average value $\overline{J_\epsilon}$ of the flux leaving the heated zone toward the center over the first 5 ms of the experiment. The detail of this calculation is given in Appendix E, which yields

$$\overline{J_\epsilon} \approx 9\,\text{mm} \cdot \text{s}^{-1}. \tag{49}$$

We consider the value of the product $(\mathbf{C} : \boldsymbol{\alpha}_{\text{th}})$ constant and can be approximated by the scalar order-of-magnitude $E \cdot \alpha_{\text{th}}$, with $E^{UO_2} \approx 200$ GPa $= 200$ J/mm^3 and $\alpha_{\text{th}}^{UO_2} \approx 10^{-5}$ K^{-1} [9].

Thus, we obtain

$$e^{5\,\mathrm{ms}}_{\mathrm{conversion}} \approx (E \cdot \alpha_{\mathrm{th}})\,\overline{J_\epsilon} \int_0^{t_f} \nabla T \cdot dt. \tag{50}$$

Evaluating the term $\int_0^{t_f} \nabla T \cdot dt$ is perhaps the most complex to establish. The first temperature profile given by Figure 1 is at 5 ms, and it is clear that thermal diffusion has already begun to establish itself. Indeed, according to [3] the laser waist used is 0.5 mm, while at 5 ms, the zone that has undergone temperature elevation has a thickness greater than 1 mm. It is therefore impossible to have an idea of the temperature gradients present around the heated zone during the first moments.

This leads us to approach the problem inversely. To estimate whether the term $e^{5\,\mathrm{ms}}_{\mathrm{conversion}}$ can legitimately account for the observed heating delay, we evaluate what order of magnitude of temperature gradient would allow us to approach the equality

$$e^{5\,\mathrm{ms}}_{\mathrm{conversion}} \approx e_{\mathrm{missing}} \approx 0.5\ \mathrm{J \cdot mm^{-3}}. \tag{51}$$

By setting $e^{5\,\mathrm{ms}}_{\mathrm{conversion}} = e_{\mathrm{missing}}$, the calculation gives an average value

$$\overline{\nabla T} \approx 5 \cdot 10^3\ \mathrm{K/mm} \tag{52}$$

for ∇T over the first 5 ms of the experiment.

This value corresponds to orders of magnitude of temperature gradient that are entirely plausible and regularly observed in the first moments of laser heating experiments. Indeed, experimental studies found in the literature generally report the range 10^3–10^4 K/mm for laser powers similar to those of the experiment in Figure 1, i.e., 620 W [22,23].

This quantitative evaluation, although based on numerous approximations, gives a promising result. It demonstrates that the order of magnitude of the influence of the coupling term $\nabla T \cdot (\mathbf{C} : \boldsymbol{\alpha}_{\mathrm{th}}) : \mathbf{J}_{\boldsymbol{\epsilon}}$ can very well correspond to the thermal energy missing during the heating experiment. Beyond the application to the laser heating experiment taken as an example, this result legitimizes the importance that must be given to this phenomenon for all experiments involving similar thermomechanical evolutions.

4. Discussion

4.1. Experimental Challenges and Quantification Perspectives

While we have provided a quantitative estimate of the strain flux $\mathbf{J}_{\boldsymbol{\varepsilon}}$ and its coupling effects during rapid transients, our approach relies on several simplifying assumptions.

The most significant limitations include the following:

- The assumption of uniform strain flux over the first 5 ms, whereas in reality it varies exponentially as mechanical equilibrium is approached;
- The approximation of isotropic material properties, while UO_2 exhibits anisotropic behavior at high temperatures;
- The indirect estimation of temperature gradients from final temperature profiles misses the critical early-stage evolution.

To overcome these limitations and provide rigorous experimental validation of the theoretical framework, direct measurement techniques are essential. Potential experimental approaches include the following:

- Laser Doppler velocimetry to measure strain rate fields in real-time [24];
- Digital image correlation for high-resolution spatio-temporal strain mapping [25];
- Time-resolved X-ray diffraction to probe local stress states during transients [26].

Crucially, given the coupling term $\nabla T \cdot (\mathbf{C} : \boldsymbol{\alpha}_{\mathrm{th}}) : \mathbf{J}_{\boldsymbol{\epsilon}}$, simultaneous measurement of both temperature gradients and strain flux is required. This necessitates combining thermal

imaging (e.g., high-speed infrared thermography) with mechanical diagnostics to capture the full thermomechanical state evolution. Only through such comprehensive experimental campaigns can the magnitude and significance of the newly identified coupling mechanism be definitively established.

4.2. Interpretation of the Observed Heating Delay

Experimental observations indicate that the initial heating delay dissipates as the system approaches steady state. A possible explanation is that a lower-than-predicted temperature gradient reduces classical conductive fluxes, partially compensating for theory–experiment discrepancies. This supports the notion that the transient strain flux $\mathbf{J}_{\boldsymbol{\varepsilon}}$ temporarily diverts energy from thermal to mechanical work.

4.3. Implications for Numerical Modeling and Applications

These findings have significant implications for numerical modeling of thermomechanical systems, particularly under rapid transient conditions. Accurately capturing these effects may require revising existing simulation codes.

Applications include the following:

- Laser heat treatment, where transient effects are critical [27];
- Additive manufacturing, where thermal gradients induce residual stresses [28,29];
- Microelectronics, where repeated thermal shocks necessitate precise transient modeling [30,31].

Understanding heat-to-mechanical-work conversion could inform process optimization and novel design strategies.

5. Conclusions

This work aims to fill a fundamental gap in thermomechanical modeling revealed by recent experiments on rapid laser heating of nuclear fuel pellets. Our main contributions and conclusions are as follows:

1. Demonstration of classical theory limitations:

- We quantitatively showed that conventional strong coupling theory can account for at most 1K temperature variation, whereas experimental discrepancies reach 150 K;
- This definitely establishes that existing frameworks cannot explain the observed heating delays.

2. Development of an extended thermomechanical framework:

- We introduced the concept of strain flux $\mathbf{J}_{\boldsymbol{\epsilon}}$ as a fundamental variable in the thermodynamics of irreversible processes;
- This approach yields a previously unknown coupling term: $\nabla T \cdot (\mathbf{C} : \boldsymbol{\alpha}_{\text{th}}) : \mathbf{J}_{\boldsymbol{\epsilon}}$;
- The new term represents mechanical work production through heat-to-work conversion during transient deformation propagation.

3. Physical interpretation and quantitative validation:

- The coupling mechanism acts as a transient heat sink during rapid thermal loading, explaining the observed heating delays;
- Our quantitative estimates show that with temperature gradients of 5×10^3 K/mm, which are common in laser heating experiments, the new coupling term can explain the missing energy density of $0.5\,\mathrm{J\,mm^{-3}}$;
- This order-of-magnitude agreement validates the relevance of the proposed mechanism.

4. Broader implications:

- The framework applies to any system experiencing rapid thermomechanical transients where $\tau_{me} \ll \tau_{th}$;
- Applications extend beyond nuclear materials to laser processing, thermal barrier coatings, and electronic packaging;
- The formalism provides a consistent bridge between classical thermoelasticity and non-equilibrium thermodynamics.

5. Future directions:

- Development of numerical schemes incorporating the strain flux conservation equation;
- Experimental campaigns combining high-speed thermography with strain field measurements;
- Extension to anisotropic materials and finite deformation regimes.

This work establishes that spatial deformation transport, long overlooked in thermomechanical coupling theory, can play a crucial role in rapid thermal transients. The proposed framework is not only capable of resolving the discrepancies observed in rapid heating experiments, but also opens up new perspectives for understanding and controlling thermomechanical processes under extreme conditions.

Author Contributions: Conceptualization, F.C., C.G. and L.D.; methodology, C.G. and L.D.; formal analysis, F.C.; writing—original draft preparation, F.C.; writing—review and editing, C.G. and L.D. All authors have read and agreed to the published version of the manuscript.

Funding: This research received no external funding.

Data Availability Statement: The original contributions presented in this study are included in the article. Further inquiries can be directed to the corresponding author.

Conflicts of Interest: The authors declare that they have no known competing financial interests or personal relationships that could have appeared to influence the work reported in this paper.

Abbreviations

The following abbreviation is used in this manuscript:

TIP Thermodynamics of Irreversible Processes

Appendix A

Choice of independent variables in the Helmholtz free energy:

Regarding Equation (6), the full expression

$$\underline{\underline{\sigma}} = \rho \frac{\partial \psi}{\partial \underline{\underline{\varepsilon}}^e} = \rho \frac{\partial \psi}{\partial \underline{\underline{\varepsilon}}} = -\rho \frac{\partial \psi}{\partial \underline{\underline{\varepsilon}}^p}, \quad s = -\frac{\partial \psi}{\partial T} \tag{A1}$$

appears in the literature [10].

However, the additional equalities follow from a particular choice of independent variables, which is generally not useful. Most often, the Helmholtz free energy is expressed as a function of the elastic strain only, $\psi = \psi(\underline{\underline{\varepsilon}}^e, T)$. Indeed, $\underline{\underline{\varepsilon}}^e$ represents the reversible part of the deformation and is the only one associated with mechanical energy storage. Furthermore, $\underline{\underline{\varepsilon}}^e$ is the true variable conjugate to the stress tensor $\underline{\underline{\sigma}}$ according to the Coleman–Noll procedure.

If one chooses the total strain $\underline{\underline{\varepsilon}}$ and the plastic strain $\underline{\underline{\varepsilon}}^p$ as independent variables, then using $\underline{\underline{\varepsilon}}^e = \underline{\underline{\varepsilon}} - \underline{\underline{\varepsilon}}^p$ one obtains

$$\left.\frac{\partial \psi(\underline{\underline{\varepsilon}}, T, \underline{\underline{\varepsilon}}^p)}{\partial \underline{\underline{\varepsilon}}}\right|_{\underline{\underline{\varepsilon}}^p, T} = \left.\frac{\partial \psi(\underline{\underline{\varepsilon}}^e, T)}{\partial \underline{\underline{\varepsilon}}^e}\right|_{T}, \quad \left.\frac{\partial \psi(\underline{\underline{\varepsilon}}, T, \underline{\underline{\varepsilon}}^p)}{\partial \underline{\underline{\varepsilon}}^p}\right|_{\underline{\underline{\varepsilon}}, T} = -\left.\frac{\partial \psi(\underline{\underline{\varepsilon}}^e, T)}{\partial \underline{\underline{\varepsilon}}^e}\right|_{T}. \tag{A2}$$

While mathematically correct, this choice of variables is not pertinent in the present context. Moreover, although ψ physically represents the same potential, it is not strictly the same function mathematically, as the set of independent variables differs.

For these reasons, it is preferable to retain the usual formulation $\psi(\underline{\underline{\varepsilon}}^e, T)$ and to remove the terms $\rho\frac{\partial \psi}{\partial \underline{\underline{\varepsilon}}} = -\rho\frac{\partial \psi}{\partial \underline{\underline{\varepsilon}}^p}$ from Equation (6), while simply noting that the Helmholtz free energy depends on the independent variables $\underline{\underline{\varepsilon}}^e$ and T.

Appendix B

Appendix B.1

Justification of the Local Equilibrium Hypothesis for Fast Transients:

It is entirely reasonable to assume local equilibrium even when studying fast transient phenomena, such as the first 5 milliseconds of the laser heating experiment. Indeed, although the transformation is very rapid, the characteristic times of microscopic phenomena, such as molecular relaxation (on the order of 10^{-12} to 10^{-10} s in crystalline solids like UO_2 [32]) and the establishment of local statistical distributions (about 10^{-14} s for phonons [33]), remain far smaller than the macroscopic timescale of our phenomenon.

Appendix B.2

Tensor Notation Conventions:

Since we work exclusively in the vector space $\mathbb{R}^3$, we adopt the following conventions:

- The tensor product is denoted $\otimes$, corresponding to the concatenation of free indices

$$(\boldsymbol{A} \otimes \boldsymbol{B})_{ijklm} = A_{ijk} B_{lm}$$

- Contracted tensor products are indicated by the following operators:
  - $\cdot$ for single contraction (over one index), for example,

$$(\boldsymbol{A} \cdot \boldsymbol{v})_i = \sum_j A_{ij} v_j$$

  - $:$ for double contraction (over two index pairs), for example,

$$(\boldsymbol{A} : \boldsymbol{B})_i = \sum_{j,k} A_{ijk} B_{jk}$$

  - $\vdots$ for triple contraction (over three index pairs), for example,

$$(\boldsymbol{A} \vdots \boldsymbol{B})_{ijp} = \sum_{k,l,m} A_{ijklm} B_{klmp}$$

- When the degree of contraction is not yet determined, the contracted product is simply denoted by $\cdot$;
- The notation $\nabla \boldsymbol{A}$ denotes the gradient of $\boldsymbol{A}$ (increasing the tensor order by 1 with the addition of a spatial index), whereas $\nabla \cdot \boldsymbol{A}$ denotes the divergence (contracting over a spatial index, thus decreasing the tensor order by 1);

- For any even integer $n \geq 2$, $\mathbb{I}^{(n)}$ denotes the identity tensor of order n. It is the element of $\mathbb{R}^{3\otimes n}$ satisfying the identity property under the $\frac{n}{2}$-fold tensor contraction. For any tensor $\boldsymbol{T}$ of compatible order, the $\frac{n}{2}$-fold contraction of $\mathbb{I}^{(n)}$ with $\boldsymbol{T}$ yields $\boldsymbol{T}$;
- For any integer $n \geq 1$, $\mathbb{O}^{(n)}$ denotes the zero tensor of order n. It is the element of $\mathbb{R}^{3\otimes n}$ whose components are all zero. For any tensor $\boldsymbol{T}$ of compatible order, any contraction of $\mathbb{O}^{(n)}$ with $\boldsymbol{T}$ gives the zero tensor of appropriate order;
- For any invertible tensor $\boldsymbol{T}$ of even order $n \geq 2$, its inverse tensor of order n is denoted $\boldsymbol{T}^{-1}$. It satisfies the inverse property under the $\frac{n}{2}$-fold tensor contraction, i.e., the contraction of $\boldsymbol{T}$ with $\boldsymbol{T}^{-1}$ yields the identity tensor $\mathbb{I}^{(n)}$;
- When necessary, detailed calculations explaining certain tensorial equalities, specifying contracted indices and methods, have been specifically provided in Appendix F.

Appendix B.3

Derivation of the Entropy Production Expression:

To derive the expression for the entropy production density, we consider the following three expressions:

$$\frac{\partial s}{\partial t} = \sum_i \frac{\partial s}{\partial \boldsymbol{x}_i} \cdot \frac{\partial \boldsymbol{x}_i}{\partial t} = \sum_i \boldsymbol{I}_i \cdot \frac{\partial \boldsymbol{x}_i}{\partial t} \tag{A3}$$

$$\mathbf{J}_s = \sum_i \frac{\partial s}{\partial \boldsymbol{x}_i} \cdot \mathbf{J}_i = \sum_i \boldsymbol{I}_i \cdot \mathbf{J}_i \tag{A4}$$

$$\frac{\partial \boldsymbol{x}_i}{\partial t} + \nabla \cdot \mathbf{J}_i = \mathbf{0} \tag{A5}$$

with the following applying:

- $\boldsymbol{x}_i$ the local thermodynamic variables of the system (tensorial or scalar quantities in the context of continuum mechanics);
- $\boldsymbol{I}_i = \frac{\partial s}{\partial \boldsymbol{x}_i}$ the intensive quantities representing the sensitivity of s to $\boldsymbol{x}_i$;
- and $\mathbf{J}_i$ the flux densities associated with the quantities $\boldsymbol{x}_i$.

Equation (A3) follows from the differential expression of $s(\boldsymbol{x}_i)$.

Equation (A4) expresses $\mathbf{J}_s$ in terms of the flux densities of the various quantities $\boldsymbol{x}_i$.

Finally, Equation (A5) recalls the conservation equation for the quantities $\boldsymbol{x}_i$.

In our case, the two irreversible processes considered are the thermal and mechanical evolutions. Based on Equation (18), the $\boldsymbol{x}_i$ that can be considered are the internal energy u and the strain tensor $\boldsymbol{\epsilon}$. The fluxes $\mathbf{J}_i$ studied are thus the energy flux density vector $\mathbf{J}_u$ (in $\mathrm{W} \cdot \mathrm{m}^{-2}$) and the strain flux tensor $\mathbf{J}_{\boldsymbol{\epsilon}}$.

The flux $\mathbf{J}_{\boldsymbol{\epsilon}}$ represents the spatial transport of local strains. Physically, this corresponds to the propagation of elastic deformations in the continuous medium. It is an order 3 tensor; each component $J_{\epsilon_{ij},k}$ represents the flux of the strain component ϵ_{ij} in the direction k. The unit of $\mathbf{J}_{\boldsymbol{\epsilon}}$ is $\mathrm{m} \cdot \mathrm{s}^{-1}$ (dilation flux in $\mathrm{m}^3 \cdot \mathrm{m}^{-2} \cdot \mathrm{s}^{-1}$). In the continuous framework considered here, this flux satisfies the local conservation equation

$$\frac{\partial \boldsymbol{\epsilon}}{\partial t} + \nabla \cdot \mathbf{J}_{\boldsymbol{\epsilon}} = \mathbb{O}^{(2)} \tag{A6}$$

where the divergence is applied to the third index of $\mathbf{J}_{\boldsymbol{\epsilon}}$.

This relation expresses that the local temporal variations in the strain are balanced by spatial transport, consistent with the interpretation of the flux as a mechanism for the propagation of elastic deformations.

Equation (19) can thus be rewritten as

$$\begin{aligned}\nu_s &= \frac{\partial s(\mathbf{r},t)}{\partial t} + \nabla\cdot\mathbf{J}_s \\ &= I_u\,\frac{\partial u}{\partial t} + \boldsymbol{I}_{\boldsymbol{\epsilon}} : \frac{\partial \boldsymbol{\epsilon}}{\partial t} + \nabla\cdot(I_u\mathbf{J}_u + \boldsymbol{I}_{\boldsymbol{\epsilon}} : \mathbf{J}_{\boldsymbol{\epsilon}}) \\ &= I_u(-\nabla\cdot\mathbf{J}_u) + \boldsymbol{I}_{\boldsymbol{\epsilon}} : (-\nabla\cdot\mathbf{J}_{\boldsymbol{\epsilon}}) + \nabla I_u\cdot\mathbf{J}_u + I_u(\nabla\cdot\mathbf{J}_u) + (\nabla\boldsymbol{I}_{\boldsymbol{\epsilon}})\vdots\mathbf{J}_{\boldsymbol{\epsilon}} + \boldsymbol{I}_{\boldsymbol{\epsilon}} : (\nabla\cdot\mathbf{J}_{\boldsymbol{\epsilon}})\end{aligned}$$

(see Appendix F.1 for the detailed equality $\nabla\cdot(\boldsymbol{I}_{\boldsymbol{\epsilon}} : \mathbf{J}_{\boldsymbol{\epsilon}}) = (\nabla\boldsymbol{I}_{\boldsymbol{\epsilon}})\vdots\mathbf{J}_{\boldsymbol{\epsilon}} + \boldsymbol{I}_{\boldsymbol{\epsilon}} : (\nabla\cdot\mathbf{J}_{\boldsymbol{\epsilon}})$)

And therefore:

$$\nu_s = \nabla I_u\cdot\mathbf{J}_u + \nabla\boldsymbol{I}_{\boldsymbol{\epsilon}}\vdots\mathbf{J}_{\boldsymbol{\epsilon}}. \tag{A7}$$

Appendix B.4

Change in Basis for Entropy Production:

In accordance with the local equilibrium hypothesis

$$\mathbf{J}_u = \mathbf{J}_q + \boldsymbol{\sigma} : \mathbf{J}_{\boldsymbol{\epsilon}}, \tag{A8}$$

where $\mathbf{J}_q (= T\,\mathbf{J}_s)$ is the heat flux (a vector), and $\boldsymbol{\sigma} : \mathbf{J}_{\boldsymbol{\epsilon}}$ is also an order 1 tensor.

As the entropy source term ν_s is independent of the chosen basis, it follows that

$$\begin{aligned}\nu_s &= \nabla\left(\frac{1}{T}\right)\cdot\mathbf{J}_u + \nabla\left(-\frac{\boldsymbol{\sigma}}{T}\right)\vdots\mathbf{J}_{\boldsymbol{\epsilon}} \\ &= \nabla\left(\frac{1}{T}\right)\cdot(\mathbf{J}_q + \boldsymbol{\sigma} : \mathbf{J}_{\boldsymbol{\epsilon}}) + \nabla\left(-\frac{\boldsymbol{\sigma}}{T}\right)\vdots\mathbf{J}_{\boldsymbol{\epsilon}} \\ &= \nabla\left(\frac{1}{T}\right)\cdot\mathbf{J}_q + \left[\nabla\left(\frac{1}{T}\right)\otimes\boldsymbol{\sigma} + \nabla\left(-\frac{\boldsymbol{\sigma}}{T}\right)\right]\vdots\mathbf{J}_{\boldsymbol{\epsilon}}\end{aligned}$$

(see Appendix F.2 for details on the equality $\nabla\left(\frac{1}{T}\right)\cdot(\boldsymbol{\sigma} : \mathbf{J}_{\boldsymbol{\epsilon}}) = \left(\nabla\left(\frac{1}{T}\right)\otimes\boldsymbol{\sigma}\right)\vdots\mathbf{J}_{\boldsymbol{\epsilon}}$)

Then, noting that $\nabla\left(\frac{\sigma}{T}\right) = \frac{1}{T}\cdot\nabla\boldsymbol{\sigma} + \nabla\left(\frac{1}{T}\right)\otimes\boldsymbol{\sigma}$, we obtain the final expression in the heat/mechanical basis.

Appendix B.5

Rewriting of the Heat Flux:

To rewrite the heat flux expression, we note that setting the strain flux $\mathbf{J}_{\boldsymbol{\epsilon}}$ to zero in its previously derived Equation (30) gives

$$\mathbf{J}_{\boldsymbol{\epsilon}} = \mathbf{L}_{\boldsymbol{\epsilon}q}\cdot\nabla\left(\frac{1}{T}\right) + \mathbf{L}_{\boldsymbol{\epsilon}\boldsymbol{\epsilon}}\vdots\left(-\frac{1}{T}\nabla\boldsymbol{\sigma}\right) = \mathbb{O}^{(3)}. \tag{A9}$$

From which it follows

$$-\mathbf{L}_{\boldsymbol{\epsilon}\boldsymbol{\epsilon}}^{-1}\vdots\mathbf{L}_{\boldsymbol{\epsilon}q}\cdot\nabla\left(\frac{1}{T}\right) = \mathbf{L}_{\boldsymbol{\epsilon}\boldsymbol{\epsilon}}^{-1}\vdots\mathbf{L}_{\boldsymbol{\epsilon}\boldsymbol{\epsilon}}\vdots\left(-\frac{1}{T}\nabla\boldsymbol{\sigma}\right) = \mathbb{I}^{(6)}\vdots\left(-\frac{1}{T}\nabla\boldsymbol{\sigma}\right), \tag{A10}$$

which simplifies to

$$\left(-\frac{1}{T}\nabla\boldsymbol{\sigma}\right) = -\mathbf{L}_{\boldsymbol{\epsilon}\boldsymbol{\epsilon}}^{-1}\vdots\mathbf{L}_{\boldsymbol{\epsilon}q}\cdot\nabla\left(\frac{1}{T}\right). \tag{A11}$$

Substituting this result back into the expression for the heat flux in Equation (29) yields

$$\left(\mathbf{J}_q\right)_{\mathbf{J}_\epsilon=\mathbf{0}} = \left(\mathbf{L}_{qq} - \mathbf{L}_{q\epsilon} \vdots \mathbf{L}_{\epsilon\epsilon}^{-1} \vdots \mathbf{L}_{\epsilon q}\right) \cdot \nabla\left(\frac{1}{T}\right) \tag{A12}$$

$$= -\frac{1}{T^2}\left(\mathbf{L}_{qq} - \mathbf{L}_{q\epsilon} \vdots \mathbf{L}_{\epsilon\epsilon}^{-1} \vdots \mathbf{L}_{\epsilon q}\right) \cdot \nabla T \tag{A13}$$

By analogy with Fourier's law, we identify the thermal conductivity tensor at zero strain flux, denoted $\boldsymbol{\kappa}_\epsilon$, which is thus defined as

$$\boldsymbol{\kappa}_\epsilon = \frac{1}{T^2}\left(\mathbf{L}_{qq} - \mathbf{L}_{q\epsilon} \vdots \mathbf{L}_{\epsilon\epsilon}^{-1} \vdots \mathbf{L}_{\epsilon q}\right). \tag{A14}$$

Accordingly, the heat flux expression can be rewritten as

$$\begin{aligned}
\mathbf{J}_q &= \mathbf{L}_{qq} \cdot \nabla\left(\frac{1}{T}\right) + \mathbf{L}_{q\epsilon} \vdots \left(-\frac{1}{T}\nabla\boldsymbol{\sigma}\right) \\
&= \left(\mathbf{L}_{qq} - \mathbf{L}_{q\epsilon} \vdots \mathbf{L}_{\epsilon\epsilon}^{-1} \vdots \mathbf{L}_{\epsilon q}\right) \cdot \nabla\left(\frac{1}{T}\right) + \mathbf{L}_{q\epsilon} \vdots \mathbf{L}_{\epsilon\epsilon}^{-1} \vdots \mathbf{L}_{\epsilon q} \cdot \nabla\left(\frac{1}{T}\right) + \mathbf{L}_{q\epsilon} \vdots \left(-\frac{1}{T}\nabla\boldsymbol{\sigma}\right) \\
&= -\frac{1}{T^2}\left(\mathbf{L}_{qq} - \mathbf{L}_{q\epsilon} \vdots \mathbf{L}_{\epsilon\epsilon}^{-1} \vdots \mathbf{L}_{\epsilon q}\right) \cdot \nabla(T) + \mathbf{L}_{q\epsilon} \vdots \mathbf{L}_{\epsilon\epsilon}^{-1} \vdots \left[\mathbf{L}_{\epsilon q} \cdot \nabla\left(\frac{1}{T}\right) + \mathbf{L}_{\epsilon\epsilon} \vdots \left(-\frac{1}{T}\nabla\boldsymbol{\sigma}\right)\right]
\end{aligned}$$

which can eventually result in the following decomposition

$$\mathbf{J}_q = \underbrace{-\boldsymbol{\kappa}_\epsilon \cdot \nabla T}_{\text{classical heat conduction}} + \underbrace{\boldsymbol{\Pi} \vdots \mathbf{J}_\epsilon}_{\text{mechanically induced heat transport}}. \tag{A15}$$

Appendix B.6

Analytical Demonstration of the Relationship Between Kinetic Coefficients:

Expressing the condition $\mathbf{J}_\epsilon = \mathbb{O}^{(3)}$ at steady state using its previously defined form in Equation (30)

$$\mathbf{J}_\epsilon = \mathbf{L}_{\epsilon q} \cdot \nabla\left(\frac{1}{T}\right) + \mathbf{L}_{\epsilon\epsilon} \vdots \left(-\frac{1}{T}\nabla\boldsymbol{\sigma}\right) = \mathbb{O}^{(3)} \tag{A16}$$

and replacing $\nabla\boldsymbol{\sigma}$ (with $\boldsymbol{\sigma}$ representing $\boldsymbol{\sigma}_{\text{me}}$) by $\mathbf{C} : \boldsymbol{\alpha}_{\text{th}} \otimes \nabla T$ from Equation (40), we obtain

$$\mathbf{L}_{\epsilon q} \cdot \nabla\left(\frac{1}{T}\right) = \frac{1}{T}\mathbf{L}_{\epsilon\epsilon} \vdots (\mathbf{C} : \boldsymbol{\alpha}_{\text{th}} \otimes \nabla T), \tag{A17}$$

which can also be rewritten as

$$-\frac{1}{T^2}\,\mathbf{L}_{\epsilon q} \cdot \nabla T = \frac{1}{T}\,(\mathbf{L}_{\epsilon\epsilon} \cdot \nabla T) : \mathbf{C} : \boldsymbol{\alpha}_{\text{th}} \tag{A18}$$

(see Appendix F.3 for details of the equality $\mathbf{L}_{\epsilon\epsilon} \vdots (\mathbf{C} : \boldsymbol{\alpha}_{\text{th}} \otimes \nabla T) = (\mathbf{L}_{\epsilon\epsilon} \cdot \nabla T) : \mathbf{C} : \boldsymbol{\alpha}_{\text{th}}$).

Finally, we derive the relation between the kinetic coefficients given in Equation (41).

Appendix C

Mechanical work production by heat-to-work conversion:

The purpose of this appendix is to provide a concise, heuristic analogy between the volumetric coupling

$$\mathcal{T}_\varepsilon(\mathbf{x}, t) \equiv \nabla T \cdot (\mathbf{C} : \boldsymbol{\alpha}_{\text{th}}) : \mathbf{J}_\varepsilon$$

and the standard thermoelectric power density used to characterize Seebeck conversion.

In thermoelectricity, the local power density produced by a Seebeck-driven electromotive field reads

$$\mathcal{P}_{\mathrm{TE}}(\mathbf{x}, t) = \mathbf{J}_e(\mathbf{x}, t) \cdot (\alpha(\mathbf{x}, t)\, \nabla T(\mathbf{x}, t)),$$

where $\mathbf{J}_e$ is the electric current density and α the Seebeck coefficient. One may interpret $\alpha \nabla T$ as an "effective electromotive field" $\mathbf{E}_{\mathrm{eff}}$, so that

$$\mathcal{P}_{\mathrm{TE}} = \mathbf{J}_e \cdot \mathbf{E}_{\mathrm{eff}}.$$

The product $\mathbf{J}_e \cdot \mathbf{E}_{\mathrm{eff}}$ is the instantaneous electrical power density exchanged between the thermal field and the electrical degrees of freedom (heat→electric work).

In strict analogy we introduce here an "effective mechanical field" $\mathbf{F}$ defined formally by

$$\mathbf{F}(\mathbf{x}, t) \;\equiv\; \nabla T(\mathbf{x}, t) \cdot (\mathbf{C} : \boldsymbol{\alpha}_{\mathrm{th}}), \tag{A19}$$

such that the thermomechanical coupling density can be written as the tensorial scalar product

$$\mathcal{T}_{\varepsilon}(\mathbf{x}, t) = \mathbf{J}_{\boldsymbol{\varepsilon}}(\mathbf{x}, t) : \mathbf{F}(\mathbf{x}, t).$$

Under this viewpoint $\mathbf{F}$ plays the role of an electromotive-like field acting on the strain-flux $\mathbf{J}_{\boldsymbol{\varepsilon}}$. And the contraction $\mathbf{J}_{\boldsymbol{\varepsilon}} : \mathbf{F}$ represents the instantaneous power density exchanged between the thermal field and mechanical (strain) degrees of freedom.

The following two clarifying remarks are in order:

- The analogy is deliberately heuristic: $\mathbf{F}$ is not an electric field but a mechanical driving field constructed from the thermoelastic coupling tensor $\mathbf{C} : \boldsymbol{\alpha}_{\mathrm{th}}$ and the thermal gradient. Its definition in Equation (A19) simply makes explicit the linear mapping that associates a temperature gradient to a conjugate mechanical field.
- As in thermoelectricity, the sign and magnitude of the local power density $\mathbf{J}_{\boldsymbol{\varepsilon}} : \mathbf{F}$ depend on the relative orientation of the flux and the field. Depending on their directions, the term may locally produce mechanical power (heat→work) or absorb it (work→heat). In the context of thermomechanical coupling, the deformation flux $\mathbf{J}_{\boldsymbol{\varepsilon}}(\mathbf{x}, t)$ originates from the thermal expansion of a heated area. Thus, it is clear that the direction of propagation of $\mathbf{J}_{\boldsymbol{\varepsilon}}(\mathbf{x}, t)$ and $\nabla T(\mathbf{x}, t)$ are opposite. Conversion therefore occurs from heat to mechanical work.

Appendix D

Collinearity of the Tensor $\mathbf{J}_{\boldsymbol{\epsilon}}$ and $\vec{d}S$:

The strain flux $\mathbf{J}_{\boldsymbol{\epsilon}}$ is a third-order tensor that represents the spatial transport of the second-order strain tensor $\boldsymbol{\epsilon}$. More precisely, it encompasses the flux vectors of all strain components ϵ_{ij}. Each component $J_{\epsilon_{ij,k}}$ describes the flux of the strain component ϵ_{ij} in the direction k, where the third index k represents the direction of propagation.

When we state that $\mathbf{J}_{\boldsymbol{\epsilon}}$ is "collinear" with $\vec{d}S$ at the cylindrical boundary, we mean that each individual flux vector $\mathbf{J}_{\epsilon_{ij}}$ (corresponding to the transport of strain component ϵ_{ij}) is collinear with the surface normal $\vec{d}S$. This collinearity arises from the physical nature of the problem: the thermal expansion of the heated annular region generates radial dilation, which drives strain propagation outward from the cylinder axis. At the free surface, this propagation is necessarily perpendicular to the boundary, hence parallel to $\vec{d}S$.

This geometric alignment allows us to simplify the surface integral in the Green–Ostrogradsky formula, reducing the tensor contraction to a scalar product between the magnitude of the strain flux and the surface area.

Appendix E

Calculation of the Average Strain Flux During the First 5 ms:

The heated annulus has radius $R = 3.5$ mm, so its perimeter is $P = 2\pi R \approx 22$ mm.

During the early transient $t \in [0, t_f]$ with $t_f = 5$ ms, the peripheral temperature increases by $\Delta T_{\text{periph}} = 170$ K. The resulting increase in the perimeter is

$$\Delta P = P\, \alpha_{\text{th}}^{\text{UO}_2}\, \Delta T_{\text{periph}}. \tag{A20}$$

Using $\alpha_{\text{th}}^{\text{UO}_2} = 1 \times 10^{-5}\ \text{K}^{-1}$,

$$\Delta P = 22\ \text{mm} \times 1 \times 10^{-5}\ \text{K}^{-1} \times 170\ \text{K} \approx 4 \times 10^{-2}\ \text{mm}. \tag{A21}$$

This corresponds to a radial increase in the pellet

$$\Delta R = \frac{\Delta P}{2\pi} \approx 6 \times 10^{-3}\ \text{mm}. \tag{A22}$$

The strain flux $\mathbf{J}_{\boldsymbol{\epsilon}}$ propagates from the heated zone toward the interior and induces deformation primarily along two principal directions: the radial direction r (change in radius ΔR) and the circumferential direction (change in perimeter Δp at each radius). Along the cylinder height, dilation is unconstrained, hence no strain propagation occurs in the axial direction.

We relate the time-integral of a representative inward strain flux to the aggregate geometric change through the scalar balance

$$\int_0^{t_f} \langle \mathbf{J}_{\boldsymbol{\epsilon}} \rangle\, dt \approx \Delta R + \int_0^{P} \frac{\Delta p}{p}\, dp. \tag{A23}$$

Note that we do not explicitly introduce the cross-sectional area through which $\mathbf{J}_{\boldsymbol{\epsilon}}$ propagates, as this area provides the two dimensions needed to convert our length measures ΔR and $\int_0^P \frac{\Delta p}{p}\, dp$ into deformation volumes, and thus cancels out in the flux calculation.

Assuming the relative circumferential dilation $\Delta p/p$ is uniform at all distances from the center and therefore equal to $\alpha_{\text{th}}^{\text{UO}_2}\, \Delta T_{\text{periph}}$, the perimeter integral reduces to $\alpha_{\text{th}}^{\text{UO}_2}\, \Delta T_{\text{periph}}\, P$. Hence,

$$\int_0^{t_f} \langle \mathbf{J}_{\boldsymbol{\epsilon}} \rangle\, dt \approx \Delta R + \alpha_{\text{th}}^{\text{UO}_2}\, \Delta T_{\text{periph}}\, P. \tag{A24}$$

Dividing by t_f gives the time-averaged magnitude

$$\overline{J_{\boldsymbol{\epsilon}}} \approx \frac{\Delta R + \alpha_{\text{th}}^{\text{UO}_2}\, \Delta T_{\text{periph}}\, P}{t_f}. \tag{A25}$$

Numerical substitution yields

$$\overline{J_{\boldsymbol{\epsilon}}} \approx \frac{6 \times 10^{-3}\ \text{mm} + 4 \times 10^{-2}\ \text{mm}}{5 \times 10^{-3}\ \text{s}} = \frac{4.6 \times 10^{-2}\ \text{mm}}{5 \times 10^{-3}\ \text{s}} \approx 9\ \text{mm} \cdot \text{s}^{-1}. \tag{A26}$$

Appendix F

Appendix F.1

Explanation of the equality:

$$\nabla \cdot (\boldsymbol{I}_{\boldsymbol{\epsilon}} : \mathbf{J}_{\boldsymbol{\epsilon}}) = (\nabla \boldsymbol{I}_{\boldsymbol{\epsilon}}) \vdots \mathbf{J}_{\boldsymbol{\epsilon}} + \boldsymbol{I}_{\boldsymbol{\epsilon}} : (\nabla \cdot \mathbf{J}_{\boldsymbol{\epsilon}})$$

The term $\nabla \cdot (\boldsymbol{I_\epsilon} : \mathbf{J_\epsilon})$ represents the divergence of the vector obtained by the double contraction of the intensive tensor $\boldsymbol{I_\epsilon}$ (second-order) with the flux $\mathbf{J_\epsilon}$ (third-order).

In index notation, $\boldsymbol{I_\epsilon} : \mathbf{J_\epsilon}$ is written as $(\boldsymbol{I_\epsilon} : \mathbf{J_\epsilon})_k = \sum_{i,j} I_{\epsilon,ij}\, J_{\epsilon,ijk}$. The divergence then applies to the index k, yielding

$$\nabla \cdot (\boldsymbol{I_\epsilon} : \mathbf{J_\epsilon}) = \sum_k \partial_k \left(\sum_{i,j} I_{\epsilon,ij}\, J_{\epsilon,ijk} \right).$$

Applying the product rule to the spatial derivatives, we obtain

$$\sum_k \partial_k \left(\sum_{i,j} I_{\epsilon,ij}\, J_{\epsilon,ijk} \right) = \sum_{i,j,k} \left(\partial_k I_{\epsilon,ij}\right) J_{\epsilon,ijk} + \sum_{i,j,k} I_{\epsilon,ij} \left(\partial_k J_{\epsilon,ijk}\right).$$

The term $\sum_{i,j,k} \left(\partial_k I_{\epsilon,ij}\right) J_{\epsilon,ijk}$ can be interpreted as the triple contraction $(\nabla \boldsymbol{I_\epsilon}) \vdots \mathbf{J_\epsilon}$. Indeed, the gradient $\nabla \boldsymbol{I_\epsilon}$ is a third-order tensor defined component-wise by $(\nabla \boldsymbol{I_\epsilon})_{ijk} = \partial_k I_{\epsilon,ij}$, and its triple contraction with $J_{\epsilon,ijk}$ gives

$$\left(\nabla \boldsymbol{I_\epsilon} \vdots \mathbf{J_\epsilon} \right) = \sum_{i,j,k} \left(\partial_k I_{\epsilon,ij}\right) J_{\epsilon,ijk}.$$

And the term $\sum_{i,j,k} I_{\epsilon,ij} \left(\partial_k J_{\epsilon,ijk}\right)$ corresponds to the double contraction $\boldsymbol{I_\epsilon} : (\nabla \cdot \mathbf{J_\epsilon})$. Indeed, one has $\sum_{i,j,k} \left[I_{\epsilon,ij} \left(\partial_k J_{\epsilon,ijk}\right) \right] = \sum_{i,j} \left[I_{\epsilon,ij} \left(\sum_k \partial_k J_{\epsilon,ijk} \right) \right]$, and equivalently,

$$\boldsymbol{I_\epsilon} : (\nabla \cdot \mathbf{J_\epsilon}) = \sum_{i,j} \left[I_{\epsilon,ij} \left(\sum_k \partial_k J_{\epsilon,ijk} \right) \right].$$

We thus finally obtain

$$\nabla \cdot (\boldsymbol{I_\epsilon} : \mathbf{J_\epsilon}) = (\nabla \boldsymbol{I_\epsilon}) \vdots \mathbf{J_\epsilon} + \boldsymbol{I_\epsilon} : (\nabla \cdot \mathbf{J_\epsilon}).$$

Appendix F.2

Explanation of the equality:

$$\nabla \left(\frac{1}{T} \right) \cdot (\boldsymbol{\sigma} : \mathbf{J_\epsilon}) = \left(\nabla \left(\frac{1}{T} \right) \otimes \boldsymbol{\sigma} \right) \vdots \mathbf{J_\epsilon}$$

The term $\nabla \left(\frac{1}{T} \right) \cdot (\boldsymbol{\sigma} : \mathbf{J_\epsilon})$ corresponds to the scalar product between the vector $\nabla \left(\frac{1}{T} \right)$ and another vector obtained via the double contraction between the second-order tensor $\boldsymbol{\sigma}$ and the third-order tensor $\mathbf{J_\epsilon}$.

In index notation, we have

$$\left(\nabla \left(\frac{1}{T} \right) \right)_k = \partial_k \left(\frac{1}{T} \right) \quad \text{and} \quad (\boldsymbol{\sigma} : \mathbf{J_\epsilon})_k = \sum_{i,j} \sigma_{ij}\, J_{\epsilon,ijk}.$$

Thus, the scalar product, obtained by contraction over the index k, is written as

$$\nabla \left(\frac{1}{T} \right) \cdot (\boldsymbol{\sigma} : \mathbf{J_\epsilon}) = \sum_k \left[\partial_k \left(\frac{1}{T} \right) \cdot \left(\sum_{i,j} \sigma_{ij}\, J_{\epsilon,ijk} \right) \right] = \sum_{i,j,k} \partial_k \left(\frac{1}{T} \right) \cdot \sigma_{ij} \cdot J_{\epsilon,ijk}.$$

On the other hand, we can observe that

$$\partial_k\left(\frac{1}{T}\right)\cdot\sigma_{ij}=\left(\nabla\left(\frac{1}{T}\right)\otimes\boldsymbol{\sigma}\right)_{ijk},$$

which allows us to write:

$$\sum_{i,j,k}\partial_k\left(\frac{1}{T}\right)\cdot\sigma_{ij}\cdot J_{\epsilon,ijk}=\left(\nabla\left(\frac{1}{T}\right)\otimes\boldsymbol{\sigma}\right)\vdots\mathbf{J}_{\boldsymbol{\epsilon}}.$$

This demonstrates the desired tensorial identity

$$\nabla\left(\frac{1}{T}\right)\cdot(\boldsymbol{\sigma}:\mathbf{J}_{\boldsymbol{\epsilon}})=\left(\nabla\left(\frac{1}{T}\right)\otimes\boldsymbol{\sigma}\right)\vdots\mathbf{J}_{\boldsymbol{\epsilon}}.$$

Appendix F.3

Explanation of the equality:

$$\mathbf{L}_{\boldsymbol{\epsilon\epsilon}}\vdots(\mathbf{C}:\boldsymbol{\alpha}_{\text{th}}\otimes\nabla T)=(\mathbf{L}_{\boldsymbol{\epsilon\epsilon}}\cdot\nabla T):\mathbf{C}:\boldsymbol{\alpha}_{\text{th}}$$

We first observe that the following identity holds

$$(\mathbf{C}:\boldsymbol{\alpha}_{\text{th}}\otimes\nabla T)_{ijk}=(\mathbf{C}:\boldsymbol{\alpha}_{\text{th}})_{ij}\cdot\partial_k T,$$

with $(\mathbf{C}:\boldsymbol{\alpha}_{\text{th}})_{ij}=\sum_{m,n}C_{ijmn}\,\alpha_{mn}$.

Therefore, the left-hand side can be written as

$$\left(\mathbf{L}_{\boldsymbol{\epsilon\epsilon}}\vdots(\mathbf{C}:\boldsymbol{\alpha}_{\text{th}}\otimes\nabla T)\right)_{abc}=\sum_{i,j,k}L_{abcijk}\cdot(\mathbf{C}:\boldsymbol{\alpha}_{\text{th}})_{ij}\cdot\partial_k T.$$

Moreover, the coefficients $L_{abcijk}\cdot\partial_k T$ can be grouped into a partial contraction of $\mathbf{L}_{\boldsymbol{\epsilon\epsilon}}$ with ∇T over the spatial index k, which results in a fifth-order tensor

$$(\mathbf{L}_{\boldsymbol{\epsilon\epsilon}}\cdot\nabla T)_{abcij}=\sum_k L_{abcijk}\cdot\partial_k T.$$

If we then contract this tensor with the second-order tensor $(\mathbf{C}:\boldsymbol{\alpha}_{\text{th}})_{ij}$, we obtain

$$((\mathbf{L}_{\boldsymbol{\epsilon\epsilon}}\cdot\nabla T):\mathbf{C}:\boldsymbol{\alpha}_{\text{th}})_{abc}=\sum_{i,j}\left(\sum_k L_{abcijk}\cdot\partial_k T\right)\cdot(\mathbf{C}:\boldsymbol{\alpha}_{\text{th}})_{ij}=\sum_{i,j,k}L_{abcijk}\cdot(\mathbf{C}:\boldsymbol{\alpha}_{\text{th}})_{ij}\cdot\partial_k T.$$

This expression matches the left-hand side

$$\left(\mathbf{L}_{\boldsymbol{\epsilon\epsilon}}\vdots(\mathbf{C}:\boldsymbol{\alpha}_{\text{th}}\otimes\nabla T)\right)_{abc}=((\mathbf{L}_{\boldsymbol{\epsilon\epsilon}}\cdot\nabla T):\mathbf{C}:\boldsymbol{\alpha}_{\text{th}})_{abc},$$

which justifies the tensorial equality

$$\mathbf{L}_{\boldsymbol{\epsilon\epsilon}}\vdots(\mathbf{C}:\boldsymbol{\alpha}_{\text{th}}\otimes\nabla T)=(\mathbf{L}_{\boldsymbol{\epsilon\epsilon}}\cdot\nabla T):\mathbf{C}:\boldsymbol{\alpha}_{\text{th}}.$$

References

1. Maitournam, H. *Matériaux et Structures Anélastiques*; Éditions de l'École polytechnique: Palaiseau, France, 2017; pp. 79–86.
2. Doblaré, M.; Doweidar, M.H. Thermomechanics. In *Constitutive Modelling of Solid Continua*; Merodio, J., Ogden, R., Eds.; Springer: Cham, Switzerland, 2020; Volume 262, pp. 53–79.
3. Reymond, M.; Sercombe, J.; Gallais, L.; Doualle, T.; Pontillon, Y. Thermo-mechanical simulations of laser heating experiments on UO_2. *J. Nucl. Mater.* **2021**, *557*, 153220. [CrossRef]
4. Santapuri, S. Thermodynamic restrictions on linear reversible and irreversible thermo-electro-magneto-mechanical processes. *Heliyon* **2016**, *2*, e00164. [CrossRef]
5. Houlsby, G.T.; Puzrin, A.M. Rate-dependent plasticity models derived from potential functions. *J. Rheol.* **2002**, *46*, 113–126. [CrossRef]
6. Collins, I.F.; Houlsby, G.T. Application of thermomechanical principles to the modelling of geotechnical materials. *Proc. R. Soc. A Math. Phys. Eng. Sci.* **1997**, *453*, 1975–2001. [CrossRef]
7. Mindlin, R.D. Micro-structure in linear elasticity. *Arch. Ration. Mech. Anal.* **1964**, *16*, 51–78. [CrossRef]
8. Aifantis, E.C. On the role of gradients in the localization of deformation and fracture. *Int. J. Eng. Sci.* **1992**, *30*, 1279–1299. [CrossRef]
9. Igata, N.; Domoto, K. Fracture stress and elastic modulus of uranium dioxide including excess oxygen. *J. Nucl. Mater.* **1973**, *45*, 317–322. [CrossRef]
10. Lemaitre, J.; Chaboche, J.L.; Benallal, A. *Mécanique des Matériaux Solides*, 3rd ed.; Dunod: Malakoff, France, 2009; pp. 56–74.
11. Pottier, N. *Physique Statistique Hors D'équilibre – Processus Irréversibles Linéaires*; CNRS; EDP Sciences: Les Ulis, France, 2007; pp. 79–93.
12. Onsager, L. Reciprocal Relations in Irreversible Processes. I. *Phys. Rev.* **1931**, *37*, 405–426. [CrossRef]
13. Onsager, L. Reciprocal Relations in Irreversible Processes. II. *Phys. Rev.* **1931**, *38*, 2265–2279. [CrossRef]
14. Tiwari, R. Magneto-thermoelastic interactions in generalized thermoelastic half-space for varying thermal and electrical conductivity. *Waves Random Complex Media* **2021**, *34*, 1795–1811. [CrossRef]
15. Tiwari, R.; Mukhopadhyay, S. On harmonic plane wave propagation under fractional order thermoelasticity: An analysis of fractional order heat conduction equation. *Math. Mech. Solids* **2015**, *22*, 782–797. [CrossRef]
16. Zwanzig, R. Memory Effects in Irreversible Thermodynamics. *Phys. Rev.* **1961**, *124*, 983–992. [CrossRef]
17. Cattaneo, C. Sur une forme de l'équation de la chaleur éliminant le paradoxe d'une propagation instantanée. *C. R. Acad. Sci.* **1958**, *247*, 431–433.
18. Vernotte, P. Les paradoxes de la théorie continue de l'équation de la chaleur. *C. R. Acad. Sci.* **1958**, *246*, 3154–3155.
19. Cherkaev, E. Internal resonances and relaxation memory kernels in composites. *Philos. Trans. R. Soc. A* **2020**, *378*, 20190106. [CrossRef]
20. Cepellotti, A.; Marzari, N. Thermal transport in crystals as a kinetic theory of relaxons. *Phys. Rev. X* **2016**, *6*, 041013. [CrossRef]
21. Goupil, C.; Seifert, W.; Zabrocki, K.; Müller, E.; Snyder, G.J. Thermodynamics of Thermoelectric Phenomena and Applications. *Entropy* **2011**, *13*, 1481–1517. [CrossRef]
22. Wasilewski, E.; Doynov, N.; Ossenbrink, R.; Michailov, V. Investigations on the thermal conditions during laser beam welding of high-strength steel 100Cr6. *Adv. Ind. Manuf. Eng.* **2023**, *6*, 100118. [CrossRef]
23. He, X.; Fuerschbach, P. W.; DebRoy, T. Heat transfer and fluid flow during laser spot welding of 304 stainless steel. *J. Phys. D Appl. Phys.* **2003**, *36*, 1388–1398. [CrossRef]
24. Wang, F.; Krause, S.; Hug, J.; Rembe, C. A Contactless Laser Doppler Strain Sensor for Fatigue Testing with Resonance-Testing Machine. *Sensors* **2021**, *21*, 319. [CrossRef] [PubMed]
25. Sutton, M.A.; Orteu, J.J.; Schreier, H. *Image Correlation for Shape, Motion and Deformation Measurements*; Springer: New York, NY, USA, 2009.
26. Radousky, H.B.; Armstrong, M.R.; Goldman, N. Time resolved X-ray diffraction in shock compressed systems. *J. Appl. Phys.* **2021**, *129*, 040901. [CrossRef]
27. Elsheikh, A.H.; Shanmugan, S.; Muthuramalingam, T.; Kumar, R.; Essa, F.A.; Ibrahim, A.M.M. Modeling of the Transient Temperature Field during Laser Heating. *Lasers Manuf. Mater. Process.* **2021**, *8*, 97–112. [CrossRef]
28. Mercelis, P.; Kruth, J.P. Residual stresses in selective laser sintering and selective laser melting. *Rapid Prototyp. J.* **2006**, *12*, 254–265. [CrossRef]
29. Luo, Z.; Zhao, Y. A survey of finite element analysis of temperature and thermal stress fields in powder bed fusion Additive Manufacturing. *Addit. Manuf.* **2018**, *21*, 318–332. [CrossRef]
30. Wang, Z.; Xue, S.; Long, W.; Wang, B.; Wang, J.; Zhang, P. Effects of Extreme Thermal Shock on Microstructure and Mechanical Properties of Au-12Ge/Au/Ni/Cu Solder Joint. *Metals* **2020**, *10*, 1373. [CrossRef]
31. Li, L.; Du, X.; Chen, J.; Wu, Y. Thermal Fatigue Failure of Micro-Solder Joints in Electronic Packaging Devices: A Review. *Materials* **2024**, *17*, 2365. [CrossRef]

32. Zhang, H.; Wang, X.; Douglas, J.F. Localization model description of diffusion and structural relaxation in superionic crystalline UO_2. *J. Chem. Phys.* **2019**, *151*, 071101. [CrossRef]
33. Togo, A.; Chaput, L.; Tanaka, I. Distributions of phonon lifetimes in Brillouin zones. *Phys. Rev. B* **2015**, *91*, 094306. [CrossRef]

Disclaimer/Publisher's Note: The statements, opinions and data contained in all publications are solely those of the individual author(s) and contributor(s) and not of MDPI and/or the editor(s). MDPI and/or the editor(s) disclaim responsibility for any injury to people or property resulting from any ideas, methods, instructions or products referred to in the content.